ChemPhysMater 3 (2024) 194–203

Contents lists available at ScienceDirect

ChemPhysMater

journal homepage: https://www.keaipublishing.com/en/journals/chemphysmater/

Development of red phosphor $Li_8CaLa_2Ta_2O_{13}:Eu^{3+}$ for WLEDs and anti-counterfeiting applications

Jingjing Ru[a,*], Fan Zeng[a,b], Bing Zhao[c], Chenqing Ye[a], Tonghui Zhong[a], Feiyun Guo[d], Jianzhong Chen[d,*]

[a] College of Chemistry and Materials, Fujian Province University Key Laboratory of Green Energy and Environment Catalysis, Ningde Normal University, Ningde 352100, China
[b] School of Environment and Resources, School of Carbon Neutral and Modern Industry, Fujian Normal University, Fuzhou 350007, China
[c] College of Information and Mechanical & Electrical Engineering, Ningde Normal University, Ningde 352100, China
[d] College of Chemistry, Fuzhou University, Fuzhou 350108, China

ARTICLE INFO

Keywords:
Phosphor
Tantalate
Luminescence
LED device

ABSTRACT

A set of novel red phosphors $Li_8CaLa_2Ta_2O_{13}:xEu^{3+}$ (LCLTO:xEu^{3+}) were successfully prepared using a solid-state reaction method. The properties of the prepared samples, including phase purity, elemental composition, and morphology, were systematically investigated using X-ray diffraction, scanning electron microscopy, and diffuse reflectance spectroscopy analyses. The 610 nm maximum emission peak is attributed to the $^5D_0 \rightarrow {}^7F_2$ transition of Eu^{3+} ion under 394 nm irradiation. Among all the LCLTO:xEu^{3+} phosphors, LCLTO:0.6Eu^{3+} showed the strongest emission intensity because of the concentration quenching effect of the electric dipole–dipole interaction among the Eu^{3+} ions, which was also demonstrated by the decay curves. Remarkably, the emission intensity of the optimal LCLTO:0.6Eu^{3+} phosphor, which exhibited a high internal quantum efficiency of 49.30% and excellent color purity of 96.79%, was approximately 2.29 times higher than that of commercial $Y_2O_3:Eu^{3+}$ red phosphors. The thermal stability of the LCLTO:0.6Eu^{3+} sample with good color stability was meticulously investigated. The fabricated white-light-emitting diode (WLED) exhibited a superior color-rendering index of $R_a = 82$ and chromaticity coordinates of (0.3260, 0.3639), suggesting that LCLTO:0.6Eu^{3+} has potential applicability in developing efficient and high-quality WLEDs. Moreover, the prepared LCLTO:0.6Eu^{3+}/PDMS composite film demonstrated exceptional flexural resistance and chemical stability, indicating considerable promise for practical anti-counterfeiting applications.

1. Introduction

With the energy crisis and the enhancement of human environmental awareness, energy materials with energy-saving and environmentally friendly characteristics have received increasing attention. Phosphor-converted white-light-emitting diodes (pc-WLEDs) have emerged in many different lighting applications and have become a research hotspot owing to their excellent performance in terms of environmental protection, light efficiency, energy consumption, and lifespan [1–5]. As important components of pc-WLED devices, phosphors have a significant impact on the color-rendering index (CRI), correlated color temperature (CCT), luminous efficiency, and thermal stability of the devices. However, because of the shortage of red phosphors that are both efficient and stable in current commercial pc-WLEDs (InGaN chip + YAG:Ce^{3+} phosphor), the relevant performance indices of white LED devices are low; this restricts the popularity of WLEDs for indoor lighting [6–9]. Therefore, red phosphors that can be effectively excited by near-UV light must be urgently developed in order to improve the quality of WLEDs.

Eu^{3+} ion, as a typical red luminescent activator, has strong $^7F_0 \rightarrow {}^5L_6$ transition absorption at ~395 nm, which is indexed to the emission of the near-ultraviolet (n-UV) chip. Meanwhile, the high integrated emission intensity ratio R ($R = I(^5D_0 \rightarrow {}^7F_2)/I(^5D_0 \rightarrow {}^7F_1)$) in most Eu^{3+}-doped compounds facilitates efficient red emission in a variety of matrices; this has been deeply studied and widely reported, for example, $Ca_3Zn_3(TeO_6)_2:Eu^{3+}$ [10], $Ca_3Y_7(BO_4)(SiO_4)_5O:Eu^{3+}$ [11], $BaY_2(MoO_4)_4:Eu^{3+}$ [12], $Gd_5Si_2BO_{13}:Eu^{3+}$ [13], $Ca_2LnHf_2(AlO_4)_3:Eu^{3+}$ (Ln = Lu, Y, Gd) [14], and $Ba_2LaTaO_6:Eu^{3+}$ [15]. The red luminescence of Eu^{3+} ions at approximately 605–620 nm (corresponding to the electric dipole (ED) transition $^5D_0 \rightarrow {}^7F_2$) is hypersensitive to the symmetrical environment. To obtain high-brightness red-light emission, the selection of the host matrix is also important.

* Corresponding authors.
E-mail addresses: jing3032357@163.com (J. Ru), j.z.chen@fzu.edu.cn (J. Chen).

https://doi.org/10.1016/j.chphma.2023.11.002
Received 13 September 2023; Received in revised form 1 November 2023; Accepted 24 November 2023
Available online 10 December 2023
2772-5715/© 2023 The Authors. Publishing Services by Elsevier B.V. on behalf of KeAi Communications Co. Ltd. This is an open access article under the CC BY-NC-ND license (http://creativecommons.org/licenses/by-nc-nd/4.0/)

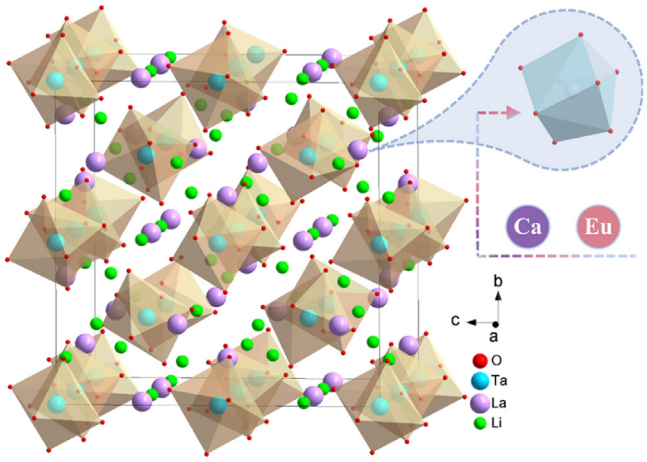

Fig. 1. Crystal structure of $Li_5La_3Ta_2O_{12}$.

Owing to its good physicochemical stability and superior luminescence properties, tantalate is considered an excellent matrix for various rare-earth-doped phosphors used in WLEDs, anti-counterfeiting applications, and latent fingerprint (LFP) detection. Hua et al. suggested that polydimethylsiloxane (PDMS) films fabricated with Ba_2LaTaO_6:Eu^{3+} phosphors are promising anti-counterfeiting materials with excellent luminescent properties and excellent flexibility [15]. Liu et al. reported that $Li_5La_3Ta_2O_{12}$:Eu^{3+} phosphors with good thermal stability (~70% of the room-temperature intensity at 423 K) are suitable for applications in WLEDs devices, except for a relatively high CCT [16]. Yu et al. proposed that $NaCaTiTaO_6$:Eu^{3+}/Sm^{3+}/Dy^{3+} phosphors could be utilized in WLED devices, achieving a high CRI (R_a) of 94, 89, and 92, respectively [17–19]. Jiao et al. suggested that the $Ca_2Ta_2O_7$:Bi^{3+} phosphor used for WLEDs exhibited a high R_a (91.1) and low CCT (3990 K) [20]. Yu et al. prepared a Ca_2InTaO_6:0.4Eu^{3+} red phosphor with excellent thermal stability (~99.9% room-temperature intensity at 420 K) and luminescence characteristics, which can be utilized for WLEDs and LFP detection [21].

However, the emission intensity of phosphors depends on the quantity of activator ions present and on the likelihood of nonradiative energy transfer occurring among these ions.

Increasing the concentration of activator ions decreases the distance between them, leading to an increased likelihood of nonradiative energy transfer and loss of emission intensity [22]. Therefore, the matrix plays a significant role in determining the quenching concentrations of the activators. For some matrices, such as the tungstate of $NaEu(WO_4)_2$ [23], molybdate of $Li_2Eu_4(MoO_4)_7$ [24], and vanadate of $Na_3Eu(VO_4)_2$ [25], Eu^{3+} ions can even replace the matrix ions completely. However, achieving high concentrations of Eu^{3+} ion doping in the reported Eu^{3+}-doped tantalate luminescent materials is rare.

The garnet-type compound $Li_5La_3Ta_2O_{12}$ crystallizes in a cubic system with the space group *Ia*-3*d*, and is widely used as a solid electrolyte material [26,27]. Recently, $Li_6CaLa_2Ta_2O_{12}$:Eu^{3+} materials were reported by Liu et al. [28]; these materials were derived from the garnet structure of $Li_5La_3Ta_2O_{12}$ by introducing Ca^{2+} ions to replace part of the La^{3+} ions with an optimal doping concentration of 50 mol% Eu^{3+} ions. As the similar ion radii and the same coordination number with La^{3+} ions (r = 1.16 Å, CN = 8), the Eu^{3+} (r = 1.07 Å, CN = 8) and Ca^{2+} (r = 1.12 Å, CN = 8) ions can be able to easily occupy the La ion sites without any alteration to the crystal structure, as shown in Fig. 1. In comparison to $Li_6CaLa_2Ta_2O_{12}$, isomorphic $Li_8CaLa_2Ta_2O_{13}$ (LCLTO) was designed with a larger interionic separation between adjacent La^{3+} ions by inserting more Li^+ ions within the crystal lattice. This structural modification is anticipated to effectively enhance the concentration of Eu^{3+} doping, thereby significantly improving the luminous efficiency [29].

Hence, LCLTO was selected as the matrix, and a series of $Li_8CaLa_{2(1-x)}Ta_2O_{13}$:$xEu^{3+}$ (LCLTO:xEu^{3+}) phosphors with high concentration Eu^{3+} doping were developed, which could be excited by near-UV light. The crystal structure and luminescence properties, including photoluminescence excitation (PLE), emission (PL), decay lifetime, thermal stability, potential applications in WLEDs, and anti-counterfeiting applications, were also examined in this study.

2. Experimental section

LCLTO:xEu^{3+} ($0.1 \le x \le 1.0$) samples were prepared via a solid-state reaction method. Specified amounts of Li_2CO_3 (99.9%), $CaCO_3$ (99.9%), La_2O_3 (99.99%), Eu_2O_3 (99.99%), and Ta_2O_5 (99.9%) were accurately weighed according to their stoichiometric ratios. Subsequently, 2 mL of ethanol was added, and the mixture was intensively ground until complete drying was achieved. When x = 0.6, 4 mmol of Li_2CO_3 (0.6780 g), 2 mmol of $CaCO_3$ (0.2088 g), 0.4 mmol of La_2O_3 (0.2719 g), 0.6 mmol of Eu_2O_3 (0.4404 g), and 1 mmol of Ta_2O_5 (0.2719 g) were added into an agate mortar, ground with ethanol for 30 min until dryness. The target products were obtained by segmented sintering. First, the mixture was pre-sintered at 450 °C for 4 h to remove the moisture from the ingredients. Subsequently, the preheated mixture was thoroughly ground and heated at 850 °C for another 5 h to break down the carbonate. Thereafter, the mixture is ground again and heated at 950 °C for 8 h to promote adequate reaction. Eventually, the target substances were obtained by grinding to a fine powder.

A schematic of the manufacturing process for LED devices and LCLTO:0.6Eu^{3+}/polydimethylsiloxane (PDMS) composite films is shown in Fig. S1. The corresponding preparation processes and characterizations are provided in Supporting Information.

3. Results and discussion

3.1. Crystal structure, phase, and morphology analysis

X-ray diffraction (XRD) patterns of the prepared LCLTO:xEu^{3+} samples are shown in Fig. 2(a). The diffraction peaks for x = 0.1–0.8 match well with the patterns calculated from ICSD database ($Li_5La_3Ta_2O_{12}$, ICSD #68252). However, two small impurity peaks (denoted by *) located at approximately 22.88° and 42.13° were detected for x > 0.9. Although the lattice structure of LCLTO:xEu^{3+} does not fundamentally change for x = 0–1, as the doping concentration of Eu^{3+} increases, the peaks gradually shift toward higher angles. For example, the strongest diffraction peaks around 34.38°–35.25° (right side of Fig. 2(a)) may be attributed to the shrinking of the lattice by the introduction of Eu^{3+} and Ca^{2+} with a smaller ion radius into the La^{3+} sites.

XRD–Rietveld refinements for the optimal sample of LCLTO:0.6Eu^{3+} were carried out using GSAS II software [28]. Fig. 2(b) shows the refinement plots, wherein the blue and orange lines represent the experimental and calculated results, respectively. The purple lines underneath indicate differences between the calculated and experimental data. The blue bars below the purple lines indicate the Bragg diffraction positions obtained from the crystal structures. The synthesized LCLTO:0.6Eu^{3+} sample crystallizes in cubic crystal system, *Ia*-3*d* space group, with the cell parameters of $a = b = c$ = 12.601 Å, $\alpha = \beta = \gamma$ = 90°, V = 2000.9 Å^3. The refined results converge to χ^2 = 3.62, R_{wp} = 7.32%, and R_p = 5.53%, indicating that the results of refinement are credible. Compared with the ICSD data of $Li_5La_3Ta_2O_{12}$ ($a = b = c$ = 12.823 Å, $\alpha = \beta = \gamma$ = 90°, V = 2108.5 Å^3), both the axial length and cell volume show a certain degree of reduction, suggesting the successful incorporation of Ca^{2+} and Eu^{3+} ions in the matrix lattice because of their smaller ionic radii relative to that of La^{3+} ions. In the LCLTO:0.6Eu^{3+} structure, the TaO_6 octahedron is located at the 16*a* Wyckoff lattice position, whereas the $(La/Ca/Eu)O_8$ dodecahedron resides at the Wyckoff lattice position of 24*c*. Notably, these two types of polyhedra were linked to each other

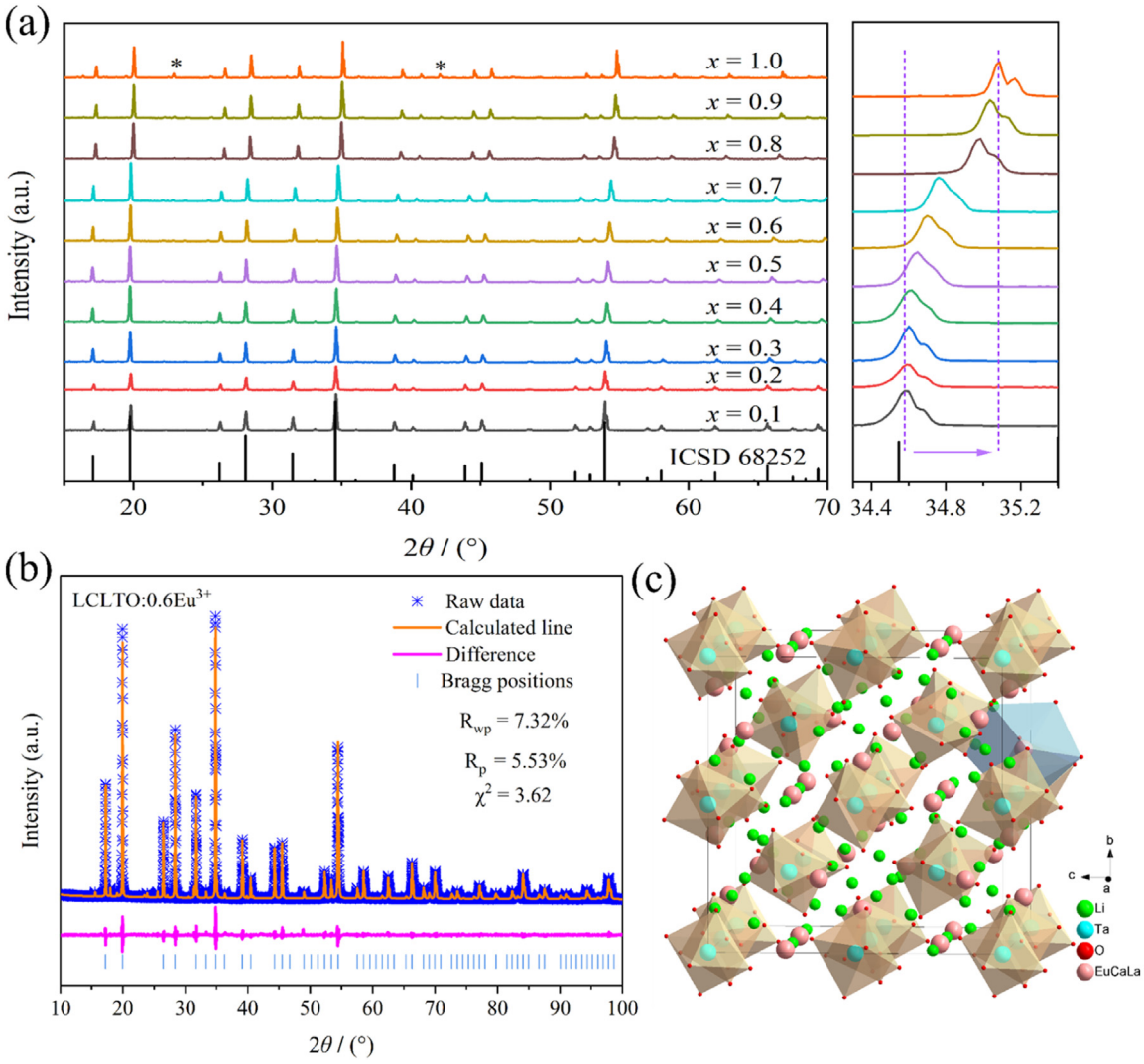

Fig. 2. XRD patterns of (a) LCLTO:xEu^{3+}, (b) Rietveld refinements for LCLTO:0.6Eu^{3+}, and (c) crystal structure of LCLTO:0.6Eu^{3+}.

through co-edge connections, forming a body-centered cubic structure, as shown in Fig. 2(c).

In general, the particle size of phosphors directly affects their performance in terms of absorption and emission efficiencies, dispersion, and color quality. An appropriate particle size ensures that these phosphors can effectively absorb the light emitted by the LED chip and convert it into the desired color. Scanning electron microscopy (SEM) images of the LCLTO:0.6Eu^{3+} samples without pretreatment are shown in Fig. 3(a). The image reveals that the sample is composed of irregular particles with sizes in the range of several microns, which is in line with LED packaging requirements. The elemental composition and homogeneity of the LCLTO:0.6Eu^{3+} samples were further confirmed via energy-dispersive spectroscopy (EDS) and elemental mapping, as shown in Figs. 3(b)–(h). The peaks for Ca, La, Eu, Ta, and O can be clearly observed in the EDS spectrum. Meanwhile, spots of different colored elements are clearly displayed on the dark background, indicating that these related elements are uniformly distributed over the particles, which further reveals that Eu^{3+} ions are successfully doped into the LCLTO lattice.

The measured atomic ratios of Ca, La, Eu, Ta, and O were 5.37%, 4.63%, 6.38%, 11.25%, and 72.38%, respectively, which are approximately equivalent to the theoretical atomic ratios of LCLTO: 0.6Eu^{3+} without considering Li atoms (theoretical values of 5.37%, 4.44%, 6.67%, 11.11%, and 72.22%, respectively). This also demonstrates that LCLTO: 0.6Eu^{3+} was smoothly synthesized.

The UV–visible (Vis) diffuse reflectance spectroscopy (DRS) spectra of the LCLTO:xEu^{3+} phosphors are shown in Fig. 4(a). The absorption intensity of the LCLTO:xEu^{3+} samples in the dotted frame region was significantly higher than that of the LCLTO matrix; this could be attributed to the overlapping charge transfer band (CTB) between the La^{3+}-O^{2-} and Eu^{3+}-O^{2-} ions. Moreover, the observed absorption peaks at 362, 380, 394, 415, 465, and 535 nm were ascribed to the characteristic absorption transition peaks of the Eu^{3+} ions introduced into the LCLTO matrix. The presence of these peaks further corroborates the accuracy of the EDS results.

Fig. 4(b) shows the PLE spectrum of LCLTO:0.6Eu^{3+} at an emission wavelength of 610 nm. The broad absorption band observed in the 230–344 nm range arises from the combined effects of charge transfer transitions between O^{2-} and metal cations within the matrix, as well as the $^7F_0 \rightarrow {}^5H_3/{}^5H_6$ transitions of Eu^{3+} ions. By using the Gaussian fitting technique, a broad band can be resolved into individual components corresponding to specific bond types. In particular, the observed absorption band can be deconvoluted into two distinct contributions, namely, the CTB of La–O bond centered at 293 nm and the one of Eu–O bond located at approximately 313 nm. A series of sharp absorption peaks at 350 and 550 nm are ascribed to the 4f-4f transitions of Eu^{3+} ions, which are arose from the $^7F_0 \rightarrow {}^5D_4$ (362 nm), $^7F_0 \rightarrow {}^5G_3$ (383 nm), $^7F_0 \rightarrow {}^5L_6$ (394 nm), $^7F_0 \rightarrow {}^5D_3$ (415 nm), $^7F_0 \rightarrow {}^5D_2$ (465 nm), and $^7F_0 \rightarrow {}^5D_1$ (534 nm), respectively [30–32]. The prominent absorption peak at 394 nm coincides well

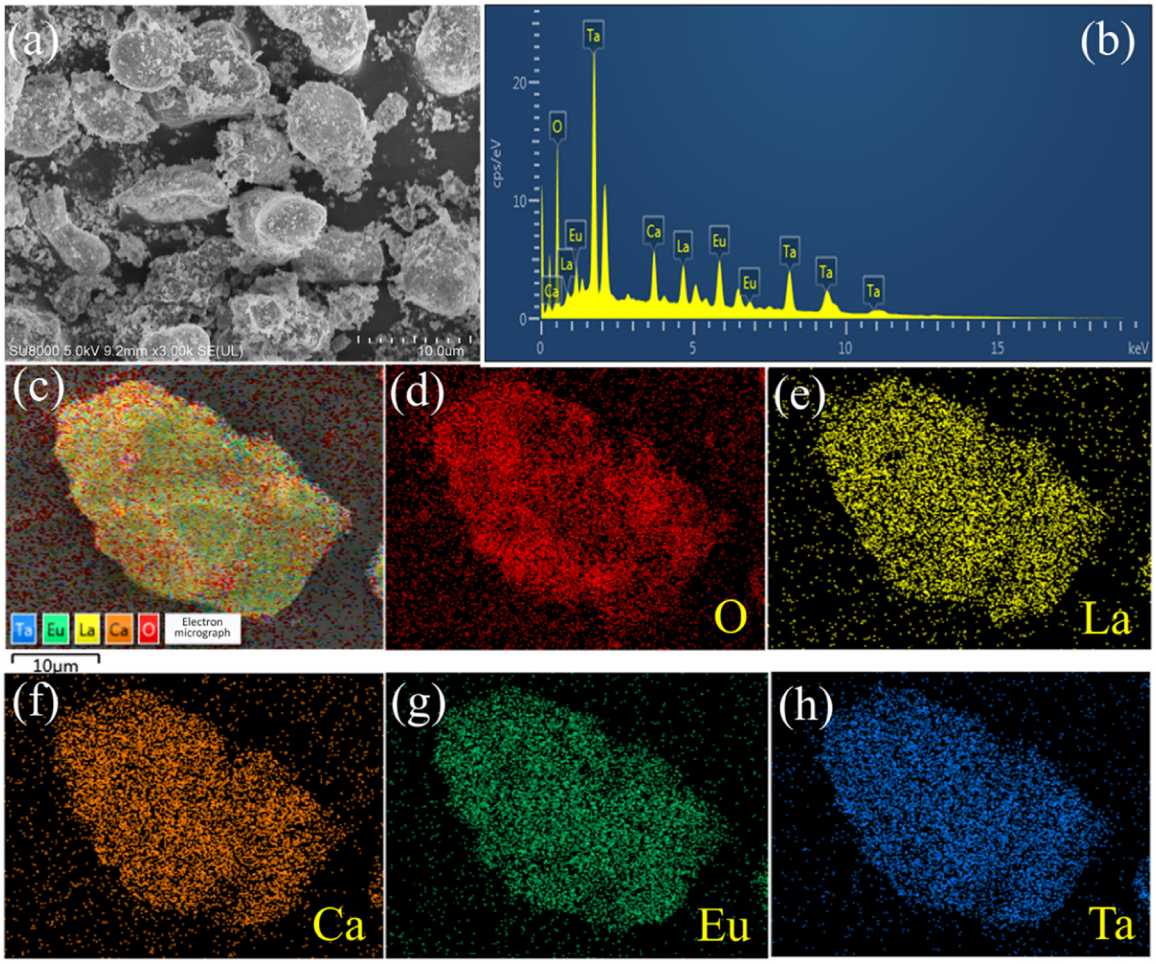

Fig. 3. (a) SEM image, (b) EDS pattern, and (c)–(h) element mappings of LCLTO:0.6Eu^{3+}.

with the near-UV light of InGaN-based LEDs, demonstrating the excellent compatibility of the LCLTO:$x$$Eu^{3+}$ phosphors in WLED devices and suggesting that these phosphors hold considerable promise for applications in solid-state lighting technology.

The PL spectra and curve depicting the relationship between the fluorescence intensity and concentration of Eu^{3+} ions are shown in Figs. 4(c)(d). Phosphors with varying Eu^{3+} doping concentrations exhibited similar spectral profiles without any wavelength shift. The luminescence intensity of the LCLTO:$x$$Eu^{3+}$ samples first increases and then decreases when x exceeds 0.6 because of concentration quenching (CQ). This phenomenon arises from the enhanced overlapping of electron clouds and increased nonradiative transition energy loss among Eu^{3+} ions with increasing Eu^{3+} doping concentration. Consequently, the intensity decreases instead of increasing when the doping ion concentration exceeds a certain level.

The critical distance (R_c) was used to elucidate the CQ mechanism and was initially calculated using the following formula [33]:

$$R_c \approx 2\left[\frac{3V}{4\Pi X_c N}\right]^{\frac{1}{3}}, \quad (1)$$

where X_c, N, and V refer to the critical content of Eu^{3+} ions (60 mol%), number of host cations, and volume of the unit cell, respectively. In the LCLTO matrix, X_c = 0.6, N = 8, and V = 2000.9 $Å^3$. Therefore, the R_c value is 9.3 Å, evidently greater than 5 Å, indicating that the exchange interaction can be neglected. Furthermore, the occurrence of radiation reabsorption necessitates a considerable degree of spectral overlap between the PLE and PL spectra, which is not feasible in LCLTO:$x$$Eu^{3+}$ samples. Hence, the energy transfer (ET) process is probably governed by an electric multipole interaction mechanism in the LCLTO:$x$$Eu^{3+}$ samples.

According to the theory by Dexter and Schulman [34], electric multipole interactions include three types depending on the Q values: the Q values are 6, 8, and 10 for dipole–dipole, dipole–quadrupole, and quadrupole–quadrupole interactions, respectively. The type of electric multipole interactions in LCLTO:Eu^{3+} can be defined using the following equation:

$$\frac{I}{x} = K\left[1+\beta x^{\frac{Q}{3}}\right]^{-1}, \quad (2)$$

where K and β are constants, and x represents the Eu^{3+} concentration. The linear regression analysis of lg$x$ versus lgI/x yielded a slope of −1.76 and R^2 value of 0.9784, resulting in a Q value of 5.28, which is close to 6. This further confirms that the dipole–dipole interaction serves as the dominant ET mechanism between the Eu^{3+} ions in the LCLTO:$x$$Eu^{3+}$ samples. Similar observations have been documented for other Eu^{3+}-doped red phosphors such as Ca_2YTaO_6:Eu^{3+} [35], $La_2W_2O_9$:Eu^{3+} [36], and Ca_2YSbO_6:Eu^{3+} [37].

The pronounced dominance red emission at approximately 610 nm in the characteristic spectral lines of Eu^{3+} ions is attributed to the ED transition of $^5D_0 \rightarrow {}^7F_2$, which is hypersensitive to the distortion of the antisymmetry [38]. In contrast, the magnetic dipole (MD) transition of $^5D_0 \rightarrow {}^7F_1$ at 592 nm is significantly weaker and less sensitive to the matrix coordination environment. This observation also suggests that the LCLTO:$x$$Eu^{3+}$ phosphors possess the potential to exhibit high-purity red-light emission, which can be beneficial for various optoelectronic and photonic applications. The asymmetry ratio ($R = I_{ED}/I_{MD}$), CIE coor-

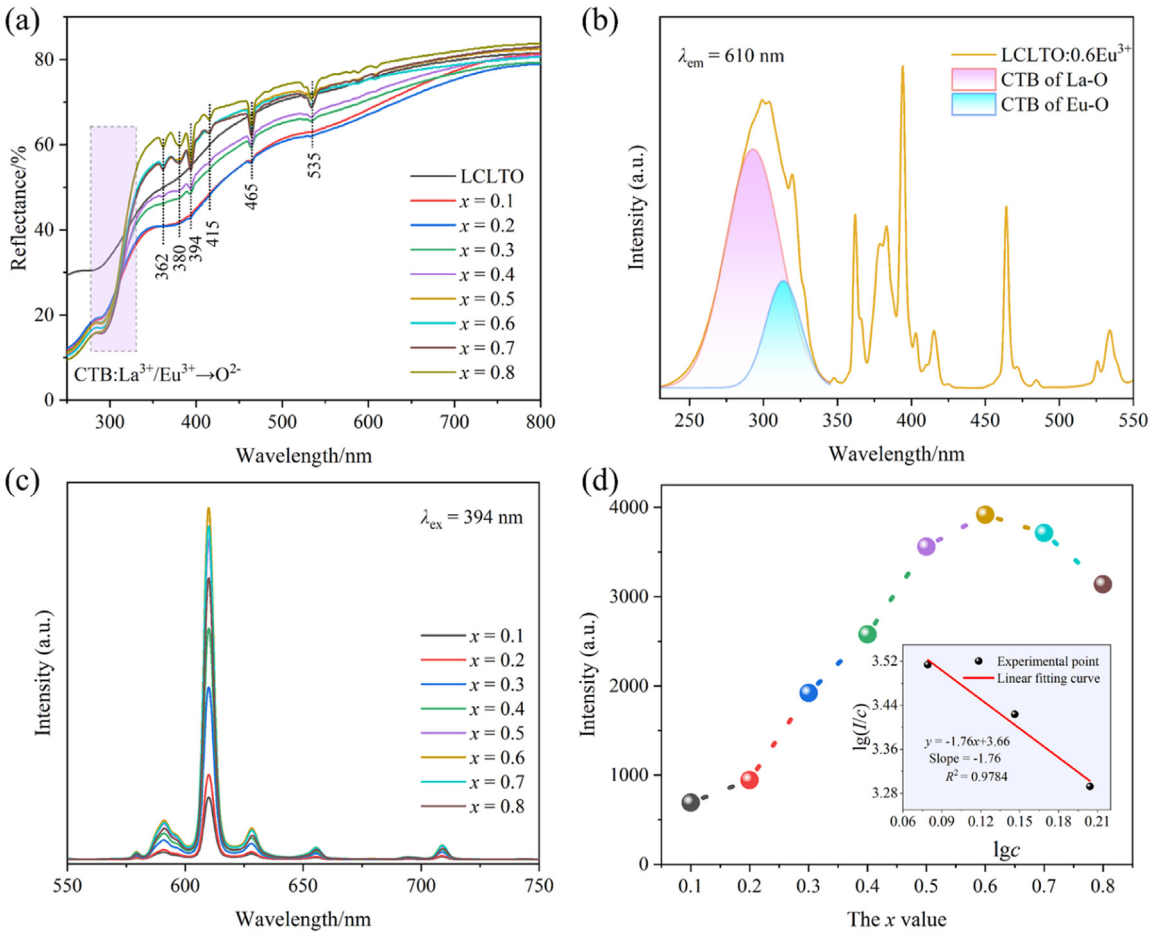

Fig. 4. (a) UV–Vis absorption spectra, (b) PLE spectrum, (c) PL spectra, and (d) relationship between emission intensity and Eu^{3+} concentration of LCLTO:xEu^{3+}.

Table 1
Asymmetry ratio R, CIE coordinates, and color purity of LCLTO:xEu^{3+} samples (λ_{ex} = 394 nm).

x value	R	CIE coordinates	Color purity (%)
0.1	8.51	(0.6370, 0.3617)	93.21
0.2	8.80	(0.6428, 0.3562)	94.80
0.3	8.83	(0.6466, 0.3527)	95.86
0.4	8.83	(0.6483, 0.3511)	96.34
0.5	8.94	(0.6495, 0.3501)	96.68
0.6	9.00	(0.6499, 0.3496)	96.79
0.7	9.04	(0.6503, 0.3493)	96.91
0.8	9.07	(0.6504, 0.3492)	96.94

dinates, and color purities of the LCLTO:xEu^{3+} phosphors are listed in Table 1.

These performance parameters are significantly better than those of some other Eu^{3+} doped phosphors. For example, in the case of LCLTO:0.6Eu^{3+}, the R value is 1.23, 2.15, 2.66, 3.6 and 4.09 times those of Ca_2YTaO_6:0.4Eu^{3+} (7.3) [39], $Ba_2Gd_{4.5}Eu_{0.5}B_5O_{17}$ (4.18) [40], $NaCa_{0.7}Eu_{0.3}TiTaO_6$ (3.38) [17], Mg_2LaTaO_6:Eu^{3+} (2.5) [41], and YBO_3:Eu^{3+} (2.2) [42], respectively. In addition, the color purity of 96.79% was higher than that of Ba_2YSbO_6:0.7Eu^{3+} (93.8%) [43], $Na_3Sc_2(PO_4)_3$:Eu^{3+} (87%) [44], Ca_2SiO_4:Eu^{3+} (91.2%) [45], and Sr_2LaTaO_6:0.15Eu^{3+} (89.2%) [46]. Additionally, the CIE chromaticity coordinates (0.6499, 0.3496) were better than those of the commercial red phosphor Y_2O_3:Eu^{3+} (0.593, 0.344), which was close to ideal red light (0.670, 0.330). A comparative analysis was performed on the PL spectra of LCLTO:0.6Eu^{3+} and Y_2O_3:Eu^{3+} under 394 nm excitation (Fig. 5(b)). The integrated PL intensity in Fig. 5(b) indicates that the strength of LCLTO:0.6Eu^{3+} was significantly higher than that of Y_2O_3:Eu^{3+} (approximately 2.29 times).

The decay curves of LCLTO: xEu^{3+} (x = 0.1, 0.2, 0.4, 0.6, 0.7, and 0.8) presented in Fig. 5(c) provide direct insight into the ET process. All curves exhibit a satisfactory fit to the single-exponential behavior, as shown in Eq. (3)[47].

$$I_t = I_0 + A\exp\left(\frac{-t}{\tau}\right), \tag{3}$$

where I_0 and I_t are the PL intensity at times t_0 and t, A is a constant, and τ denotes the decay lifetime. The fitted decay lifetimes of LCLTO:xEu^{3+} were 0.638, 0.634, 0.617, 0.597, 0.548, and 0.529 ms for x = 0.1, 0.2, 0.4, 0.6, 0.7, and 0.8, respectively. The gradual reduction in the decay lifetimes is directly indicative of the enhanced nonradiative interactions with increasing Eu^{3+} concentration.

A high internal quantum efficiency (IQE) for phosphors holds remarkable practical significance in various applications as they can efficiently convert absorbed light energy into emitted photons up to the hilt. This minimizes energy loss, which is affected by various factors such as the properties of the matrix material, morphology, dopant ions, and excimer formation[48,49]. The IQE (η) of the LCLTO:0.6Eu^{3+} was calculated using the following equation[50]:

$$\eta = \frac{\int L_S}{\int E_R - \int E_S}, \tag{4}$$

where L_S is the emission spectrum of the sample, and E_R and E_S are the excitation spectra without and with the sample, respectively. The IQE of LCLTO:0.6Eu^{3+} under 394 nm excitation was calculated to be 49.30% (as illustrated in Fig. 5(d)), which is compara-

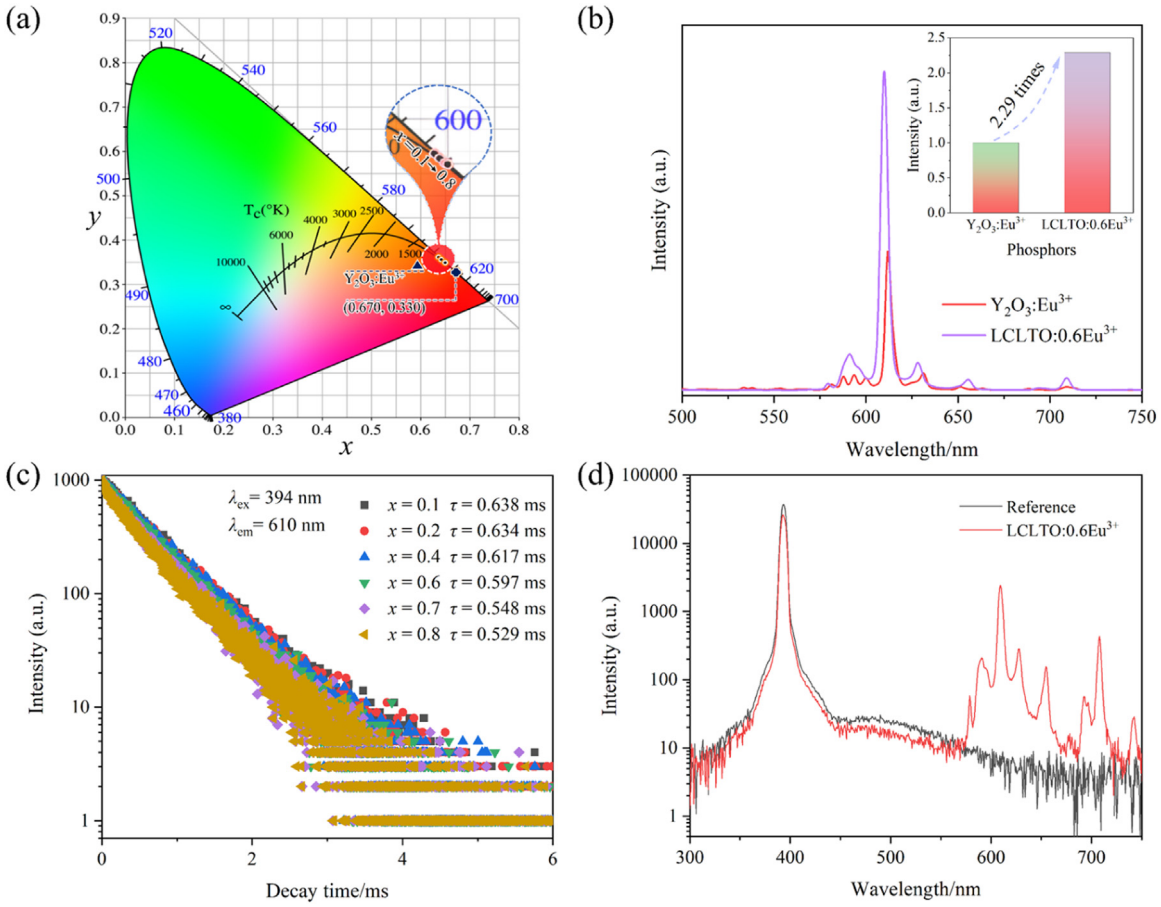

Fig. 5. (a) CIE coordinate of LCLTO:xEu^{3+}, (b) PL spectra of Y_2O_3:Eu^{3+} and LCLTO:0.6Eu^{3+}, (c) decay curves of LCLTO:0.6Eu^{3+}, and (d) PLE line of $BaSO_4$ and PL spectrum of LCLTO:0.6Eu^{3+}.

ble to those of Ca_2GdNbO_6:0.1Eu^{3+}(49.39%) and Ca_2LaNbO_6:0.1Eu^{3+} (42.96%) and much higher than those of Ca_2LaSbO_6:0.1Eu^{3+} (19.23%), Ca_2GdSbO_6:0.1Eu^{3+} (20.76%), and Ca_2YSbO_6:0.1Eu^{3+} (24.85%) [51]. However, there remains a disparity with regard to the IQE of Y_2O_3:Eu^{3+} (63.40%, as shown in Fig. S2).

Typically, LEDs generate a considerable amount of heat during their operation, with temperatures reaching approximately 420 K. Therefore, it is crucial for the phosphors used in pc-WLEDs to possess high thermal stability so that their luminescent properties and color stability can be maintained at high temperatures. This is imperative to ensure that the emission efficiency and color quality of the LEDs remain unperturbed. The temperature-dependent PL spectra of the LCLTO:0.6Eu^{3+} sample in the temperature range of 300–480 K under 394 nm excitation are shown in Fig. 6. The PL intensity shows a monotonic decrease because of the thermal quenching and the 610 nm emission retains approximately 80.52% at 420 K of the value at 300 K. This is comparable to the observations in the case of $Ca_2BB'O_6$ (B = Y, Gd, La; B′ = Sb, Nb)[51], as shown in Fig. 6(a). The contour map depicting the correlation between the temperature and PL spectra, as shown in Fig. 6(b), indicate that the red position of the strongest emission peak at 610 nm barely shifts as the temperature gradually increases. The CIE coordinates (x, y) at different temperatures varied from (0.6448, 0.3540) to (0.6355, 0.3627); the CIE x and y only show a difference of 0.0093 and 0.0087, respectively, indicating that the material has good color stability. The color coordinates at 300 K (0.6448, 0.3540) obtained from the variable-temperature PL test differed slightly from the values of the LCLTO:0.6Eu^{3+} sample (0.6499, 0.3496) listed in Table 1; this can be attributed to the use of a different mold compared to that employed at room temperature.

The Arrhenius-type activation model [52] was employed to estimate the activation energy (E_a) and validate the thermal quenching mechanism of the LCLTO:0.6Eu^{3+}.

$$\ln\left(\frac{I_0}{I}-1\right)=\ln A-\frac{E_a}{k_BT}, \tag{5}$$

where I_0 and I represent the PL intensities of LCLTO:0.6Eu^{3+} at the initial and subsequent temperatures, respectively. A is a constant, and k_B is Boltzmann's constant. Thus, the slope of the fitted line for $\ln(I_0/I-1)$ and $(k_BT)^{-1}$ is estimated to be −0.17 with R^2 = 0.985, derived as 0.17 eV for E_a. This is comparable to those observed in numerous Eu^{3+}-doped phosphors, including $Na_2Y_2B_2O_7$:Eu^{3+} (0.16 eV)[53], Ca_2LaTaO_6:Eu^{3+} (0.17 eV) [54], CaLaMgSbO$_6$:Eu^{3+} (0.173 eV) [55] and $BaZrGe_3O_9$:Eu^{3+} (0.175 eV) [56], demonstrating the good thermal stability of the LCLTO:0.6Eu^{3+} sample.

The energy-level diagram and thermal quenching process are illustrated in Fig. 7. Under excitation by n-UV light at 394 nm, the electrons were excited from the ground state $^7F_0$ to the $^5L_6$ level. At lower temperatures, the majority of electrons relax to the $^5D_0$ level via nonradiative transitions, which is followed by a radiative transition back to the different ^7F_J (J = 1, 2, 3, 4) levels because of the large energy gap between the CTB of O^{2-}-Eu^{3+} and the $^5D_0$ level of Eu^{3+} ions in LCLTO:xEu^{3+} (approximately 15556 cm^{-1}), as shown in Fig. 7(a). However, as the temperature increases, the luminescent center of Eu^{3+} is thermally activated. Further, some excited electrons at the $^5D_0$ level can overcome the energy barrier with the help of phonons and jump into the CTB of O^{2-}-Eu^{3+} after absorbing thermal energy, resulting in an increase in the probability of nonradiative transitions, thus showing a decrease in the PL intensity (Fig. 7(b)).

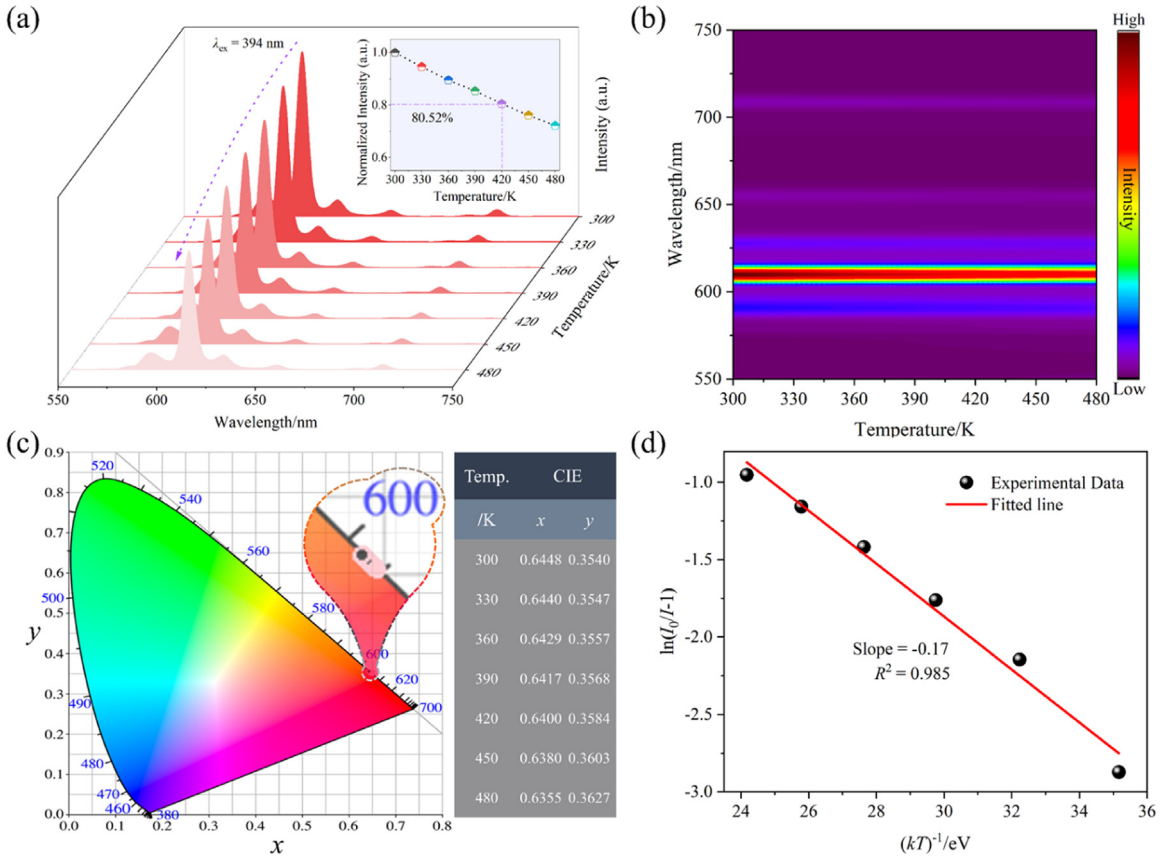

Fig. 6. (a) Temperature-dependent PL spectra, (b) contour map, (c) CIE chromaticity diagram considering different temperatures, and (d) linear fitting of $\ln(I_0/I-1)$ versus $(kT)^{-1}$ of LCLTO:0.6Eu^{3+} sample.

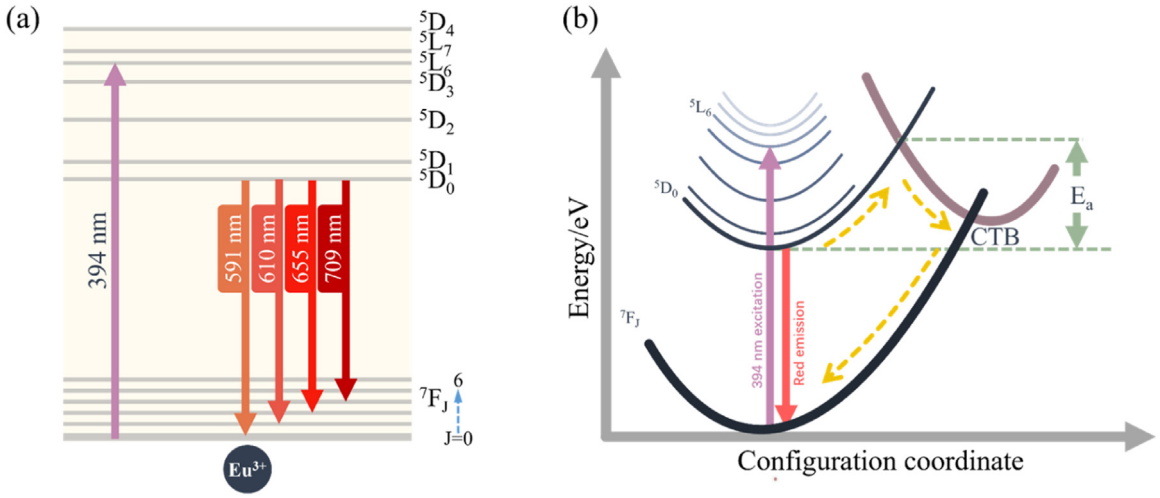

Fig. 7. (a) Energy-level diagram of $Eu^{3+}$and (b) thermal quenching mechanism of LCLTO:0.6Eu^{3+} phosphor.

The EL spectra of the packaged red LED and WLED devices with the prepared LCLTO:0.6Eu^{3+} are shown in Fig. 8. Operating at a current of 120 mA, the red LED device emitted bright red light, which is consistent with the PL spectrum of the LCLTO:0.6Eu^{3+} phosphor with chromaticity coordinates of (0.6267, 0.3324) and a CCT of 1011 K. Fig. 8(b) shows the bright white light emission of the WLED device composed of BAM:Eu^{2+}, BBS:Eu^{2+}, and LCLTO:0.6Eu^{3+} phosphors in a weight ratio of 3:1:8, driven by a current of 100 mA. CRI is an essential metric used to evaluate the ability of a WLED to render colors accurately and vividly. The higher the CRI value, the better would be the color-rendering performance. The full set of 14 CRIs and R_a values of both the prepared WLED device and the commercial device (YAG:Ce^{3+} + blue chip) are listed in Table 2. Notably, R_a represents the average color fidelity of the light source, whereas R_9 corresponds to a specific red color rendition. The WLED fabricated with the LCLTO:0.6Eu^{3+}phosphor exhibited better R_a (82) and R_9 (74) values than those of the commercial phosphor (R_a = 80, R_9 =14). The CCT of the obtained WLED device was 5757 K, which is lower than that of the commercial device (CCT = 7756 K)[57]. The luminous efficacy of the fabricated WLED was 13.3 lm/W. Moreover, the CIE coordinates (0.3260, 0.3639) of the fabricated WLED are located

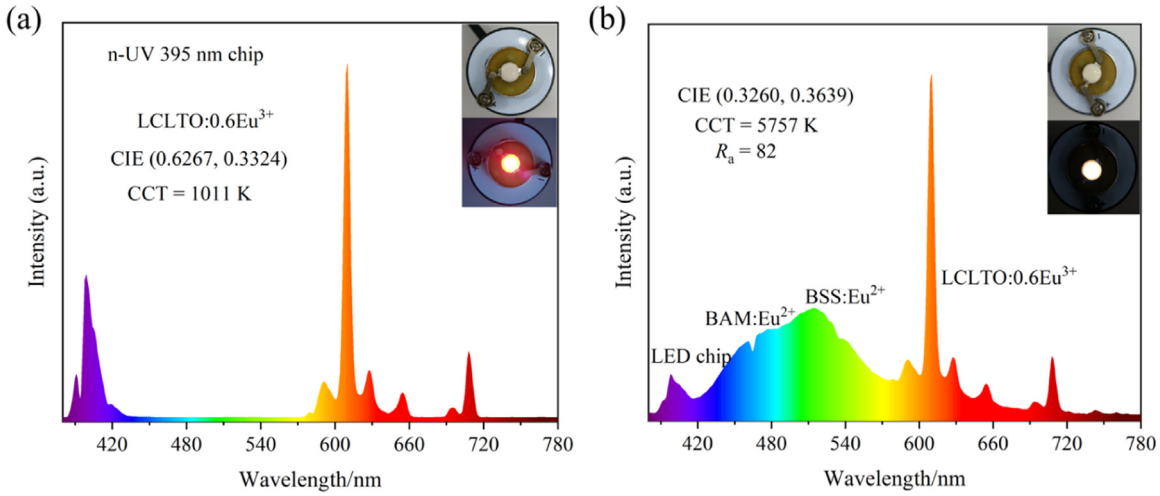

Fig. 8. (a) EL spectra of the red LED with LCLTO:0.6Eu^{3+}and (b) the constructed w-LED.

Table 2
Full set of the 14 CRIs and R_a of the fabricated and commercial WLED.

WLED	R_1	R_2	R_3	R_4	R_5	R_6	R_7	R_8	R_9	R_{10}	R_{11}	R_{12}	R_{13}	R_{14}	R_a
fabricated	81	85	84	80	83	75	86	82	61	65	74	79	80	91	82
commercial	82	83	77	84	80	72	87	77	15	55	83	45	84	84	80

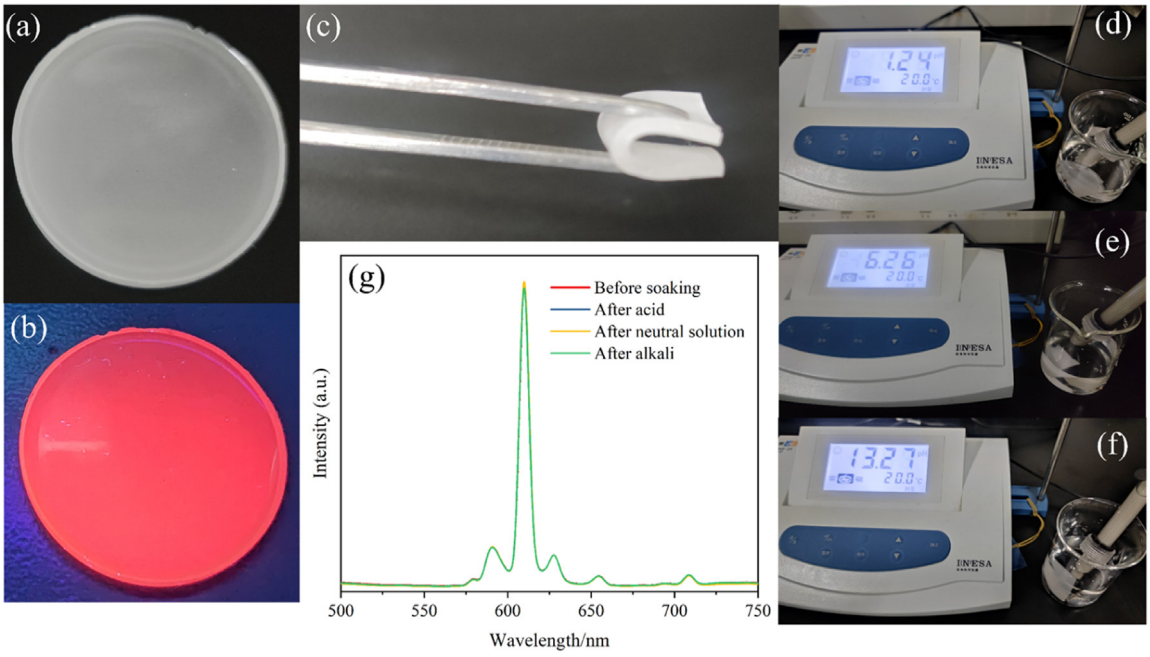

Fig. 9. Photographs of LCLTO:0.6Eu^{3+}/PDMS (a) under day light, (b) under UV light, (c) after bending test, (d)–(f) after immersing in different pH solutions, and (g) PL spectra of LCLTO:0.6Eu^{3+}/PDMS before and after different immersion treatment.

in the white region and close to the equal-energy point (0.333, 0.333). The enhanced CRI, improved R_9 values, and ideal CIE coordinates indicate that the LCLTO:0.6Eu^{3+} phosphors have potential applicability in developing efficient and high-quality WLEDs.

The procedure for preparing the LCLTO:0.6Eu^{3+}/PDMS composite films is shown in Fig. 9. The prepared composite film exhibited a white color under natural light. When excited by 365 nm UV light, the composite film emitted bright red light, as shown in Figs. 9(a)(b). In addition, the LCLTO:0.6Eu^{3+}/PDMS film demonstrated excellent flexural resistance, as it remained intact even after being subjected to bending forces (Fig. 9(c)). Figs. 9(d)–(f) present the immersion of the composite film in solutions of different pH values. After a 24 h immersion period, no significant changes were observed on the surface of the composite film, indicating the excellent chemical stability of the prepared film. Surprisingly, the emission spectra of the immersed composite film did not show a noticeable decrease in the luminescence intensity compared to that of the initial composite film (Fig. 9(g)). This is indicative of its promising potential for anti-counterfeiting applications in complex practical environments.

4. Conclusions

In summary, a series of red phosphors $Li_8CaLa_2Ta_2O_{13}$:xEu^{3+} (LCLTO:xEu^{3+}) were successfully prepared using a solid-state reaction method. XRD, SEM, EDS, DRS, PLE, PL, and decay lifetimes were measured for the LCLTO:xEu^{3+} samples. Upon 394 nm excitation, the LCLTO:xEu^{3+} samples exhibit a maximum emission peak at 610 nm, corresponding to the $^5D_0 \rightarrow {}^7F_2$ transition of Eu^{3+} ion. The optimal doping concentration of Eu^{3+} ions is x = 0.6 because of CQ. The PL intensity of the synthesized LCLTO:0.6Eu^{3+} phosphor was approximately 2.29 times greater than that of commercially available Y_2O_3:Eu^{3+} red phosphors, and the IQE and color purity of this sample reached 49.30% and 96.79%, respectively. Moreover, the LCLTO:0.6Eu^{3+} phosphor exhibited excellent thermal and color stabilities with E_a = 0.17 eV. The fabricated WLED exhibited excellent CRI (82) and CIE chromaticity coordinates (0.3260, 0.3639). These results reveal that LCLTO:0.6Eu^{3+} has potential applicability in the domain of WLEDs. Furthermore, the excellent flexural resistance and chemical stability exhibited by the prepared LCLTO:0.6Eu^{3+}/PDMS composite film suggest its promising potential for anti-counterfeiting applications in practical settings.

Declaration of Competing Interest

The authors declare that they have no known competing financial interests or personal relationships that could have appeared to influence the work reported in this paper.

CRediT authorship contribution statement

Jingjing Ru: Writing – original draft, Writing – review & editing, Formal analysis, Data curation, Investigation, Methodology. **Fan Zeng:** Data curation, Investigation. **Bing Zhao:** Software, Visualization. **Chenqing Ye:** Conceptualization, Validation. **Tonghui Zhong:** Data curation, Investigation. **Feiyun Guo:** Methodology, Visualization, Formal analysis. **Jianzhong Chen:** Methodology, Writing – review & editing.

Acknowledgements

This work was supported by the Foundation of Fujian Province (No. 2021J011149), the financial support of Innovative Research Team of Ningde Normal University (No. 2023T03), and Fujian Provincial Department of Education (No. JAT210469).

Supplementary materials

Supplementary material associated with this article can be found, in the online version, at doi:10.1016/j.chphma.2023.11.002.

References

[1] Z.Y. Cao, S.J. Dong, S.K. Shi, J.Y. Wang, L.S. Fu, Solid state reaction preparation of an efficient rare-earth free deep-red Ca_2YNbO_6:Mn^{4+} phosphor, J. Solid State Chem. 307 (2022) 122840.
[2] B. Han, X. Yang, J. Ren, L. Liu, E. Zhao, X. Zhu, J. Zhu, H. Ma, A. Li, P. Teng, Thermally stable deep-red emitting Sr_2GdTaO_6:Mn^{4+} double perovskites for indoor plant growth LEDs, Mater. Today Chem. 23 (2022) 100737.
[3] C. Yang, C.L. Fan, F. Hussain, W.Q. Sheng, K.X. Song, J. Wu, Q.M. Huang, W.T. Su, J.M. Xu, S.K. Sun, D.W. Wang, Luminescent ionic lattice occupation and wide tunable emission spectra of La_2MgZrO_6:Bi^{3+}, Eu^{3+} double perovskite phosphors for white light LED, J. Rare Earths 41 (2023) 489–497.
[4] Q.S. Wu, Y.Y. Li, Y.J. Wang, H. Liu, S.S. Ye, L. Zhao, J.Y. Ding, J.C. Zhou, A novel narrow-band blue-emitting phosphor of Bi^{3+}-activated $Sr_3Lu_2Ge_3O_{12}$ based on a highly symmetrical crystal structure used for WLEDs and FEDs, Chem. Eng. J. 401 (2020) 126130.
[5] E. Erol, N. Vahedigharehchopogh, O. Kibrisli, M.C. Ersundu, A.E. Ersundu, Recent progress in lanthanide-doped luminescent glasses for solid-state lighting applications-a review, J. Phys. Condens. Matter 33 (2021) 483001.
[6] S.K. Hussain, H.S. Go, J.J. Han, H. Patnam, G. Nagaraju, J.S. Yu, Energy transfer mechanism and tunable emissions from $K_3La(VO_4)_2$:Dy^{3+}/Eu^{3+} phosphors and soft-PDMS-based composite films for multifunctional applications, J. Alloys Compd. 805 (2019) 1271–1281.
[7] J.Y. Ding, Y. Wei, W.Q. Liu, Y.Y. Li, Q.S. Wu, J.C. Zhou, Highly efficient and thermally stable narrow-band cyan-emitting aluminum oxynitride phosphor for WLEDs and FEDs, Chem. Eng. J. 403 (2021) 126382.
[8] K. Park, D.A. Hakeem, D.H. Kim, G.W. Jung, S.W. Kim, Synthesis and photoluminescence properties of new garnet-type red-emitting $Li_7La_{3-x}Zr_2O_{12}$:xEu^{3+} phosphors, Scr. Mater 179 (2020) 92–98.
[9] H.X. Liao, M. Zhao, M.S. Molokeev, Q.L. Liu, Z.G. Xia, Learning from a mineral structure toward an ultra-narrow-band blue-emitting silicate phosphor $RbNa_3(Li_3SiO_4)_4$:Eu^{2+}, Angew. Chem. Int. Ed. 57 (2018) 11728–11731.
[10] R.P. Cao, Z.Y. Huang, B. Lan, L. Li, X.H. Yi, Z.Y. Luo, C.X. Liao, J. Wang, Adjustable luminescence properties of Eu^{3+} and Bi^{3+} codoped $Ca_3Zn_3Te_2O_{12}$ phosphor, Mater. Res. Bull. 152 (2022) 111851.
[11] T. Tian, W. Liu, Q. Liu, Y. Zhang, Y.Q. Chu, G. Liu, J.Y. Xu, A new oxyapatite red phosphor Eu^{3+}-doped $Ca_3Y_7(BO_4)(SiO_4)_5O$: Synthesis, structure and luminescence properties, J. Rare Earths 40 (2022) 709–716.
[12] R. Krishnan, R.E. Kroon, H.C. Swart, Charge transfer characteristics and luminescence properties of Eu^{3+} activated Ba_2YMoO_6 and $BaY_2(MoO_4)_4$ phosphors, Mater. Res. Bull. 145 (2022) 11554.
[13] Y.K. Liu, Y.A. Liu, H.J. Yu, C.H. Yang, C.A. Xie, J. Chen, Enhanced luminescence efficiency and thermal stability via introduction of non-rare earth Bi^{3+} in $Gd_5Si_2BO_{13}$:Eu^{3+}, J. Rare Earths 41 (2023) 989.
[14] N. Ma, W. Li, X.Y. Synthesis, crystal structure, and characterizations of Eu^{3+}-activated $Ca_2LnHf_2(AlO_4)_3$ (Ln = Lu, Y and Gd) red-emitting phosphors for phosphors-converted white LEDs, J. Lumin. 265 (2024) 120232.
[15] Y. Hua, T. Wang, J.S. Yu, P. Du, Tailoring of strong orange-red-emitting materials for luminescence lifetime thermometry, anti-counterfeiting, and solid-state lighting applications, Mater. Today Chem. 25 (2022) 100945.
[16] B. Liu, K. Wang, J.K. Li, Z.M. Liu, The synthesis and luminescent properties of Eu^{3+} doped $Li_5La_3Ta_2O_{12}$ garnet phosphor with enhanced red emission and thermally stable, J. Solid State Chem. 305 (2022) 122658.
[17] P.F. Sun, Y.F. Zhong, Z.X. Li, B.T. Liu, T.B. Li, B. Deng, R.J. Yu, Luminescence properties of novel Eu^{3+}-doped tantalate $NaCaTiTaO_6$ red-emitting phosphors for solid-state lighting, J. Am. Ceram. Soc. 102 (2019) 6077–6086.
[18] S. Shu, Y. Wang, Y.E. Ke, B. Deng, R.X. Liu, Q.Y. Song, J.X. Wang, R.J. Yu, $NaCaTiTaO_6$:Sm^{3+}: A novel orange-red-emitting tantalate phosphor with excellent thermal stability and high color purity for white LEDs, J. Alloys Compd. 848 (2020) 156359.
[19] J. Guo, S.C. Li, J.Y. Kong, Y.X. Li, L. Zhou, L.Y. Lou, Q.Y. Lv, R. Tang, L.L. Zheng, B. Deng, R.J. Yu, Synthesis and characterization of a new double perovskite phosphor: $NaCaTiTaO_6$:Dy^{3+} with high thermal stability for w-LEDs application, Opt. Laser Technol. 155 (2022) 108347.
[20] M.M. Jiao, W.Z. Sun, Y.H. Wang, S.F. Zhang, Q.F. Xu, L.C. Zhang, D.H. Wang, C.L. Yang, Luminescence property improvement and controllable color regulation of a novel Bi^{3+} doped $Ca_2Ta_2O_7$ green phosphor through charge compensation engineering and energy transfer, Phys. Chem. Chem. Phys. 23 (2021) 25886.
[21] X. Ouyang, R.Y. Liu, X.P. Hu, J. Li, R. Tang, X.Y. Jin, S.G. Chen, X.M. Yao, B. Deng, H.L. Geng, R.J. Yu, Preparation, characterization, and application of a red phosphor Ca_2InTaO_6:Eu^{3+} in w-LEDs and latent fingerprint detection, J. Alloys Compd. 939 (2023) 168715.
[22] B. Han, B.B. Liu, J. Zhang, Y.Z. Dai, H.Z. Shi, $NaKLaNbO_5$:Eu^{3+}: A highly efficient and thermally stable orange-red emitting phosphor for white light-emitting diodes, J. Lumin. 212 (2019) 99–105.
[23] A.K. Munirathnappa, V.C. Petwal, J. Dwivedi, N.G. Sundaram, Enhanced red luminescence and improved crystallinity in $NaEu(WO_4)_2$ phosphors: An electron beam irradiation study, New J. Chem. 42 (2018) 2726–2732.
[24] J.J. Ru, S.M. Ying, W.X. Zheng, J.Z. Chen, A promising red-emitting phosphor $Li_2Eu_4(MoO_4)_7$ prepared by sol-gel method, Mater. Res. Bull. 84 (2016) 468–473.
[25] J.C. Zhou, Y.L. Zhang, Y. Yao, B. Wang, Y.Q. Lai, X.T. Huang, Q.S. Wu, High-efficiency fully concentrated $Na_3Eu(VO_4)_2$ phosphor with excellent thermal stability for white light-emitting diodes, J. Mater. Sci. Mater. Electron. 31 (2020) 12872–12879.
[26] N. Hamao, Y. Yamaguchi, K. Hamamoto, Low-temperature synthesis of dense garnet-type $Li_{6.5}La_3Zr_{1.5}Ta_{0.5}O_{12}$ layered structures using fluorite-type precursor oxide, J. Alloys Compd. 865 (2021) 158223.
[27] J.P. Smith, K.E. Sickafus, C.J. Rawn, C. Delzer, C.F. Chen, C. Melcher, Thermal processing conditions for the synthesis of near theoretical density $Li_5La_3Ta_2O_{12}$ ceramics for ceramic dual-mode detectors, J. Alloys Compd. 872 (2021) 159714.
[28] F.X. Liu, Y.Z. Fang, N. Zhang, J.S. Hou, Z.F. Ma, G.Y. Zhao, Blue light excited $Li_6CaLa_2M_2O_{12}$:Eu^{3+} (M=Ta, Sb) red-emitting phosphors: Structure and photoluminescence properties, Ceram. Int. 40 (2014) 14781–14786.
[29] D.L. Wei, H.J. Seo, $Li_8CaRE_2Ta_2O_{13}$ (RE=La^{3+}, Eu^{3+}, Gd^{3+}, Dy^{3+}, Er^{3+}, Y^{3+}, Yb^{3+}): A highly lithium-stuffed tantalate garnet with versatile luminescence characteristics, J. Alloys Compd. 826 (2020) 154186.
[30] R. Krishnan, R.E. Kroon, H.C. Swart, Charge transfer characteristics and luminescence properties of Eu^{3+} activated Ba_2YMoO_6 and $BaY_2(MoO_4)_4$ phosphors, Mater. Res. Bull. 145 (2022) 111554.
[31] R.P. Cao, H. Liang, T. Chen, Z.Y. Wu, Z.Y. Jiang, X.H. Yi, J.P. Wen, Q.H. Zhong, Study on luminescence characterizations of $SrMg_2La_2W_2O_{12}$:Eu^{3+} red-emitting phosphor, J. Phys. Chem. Solids 163 (2022) 110569.
[32] X.Y. Shi, M.H. Zhang, X.Y. Lu, Q.N. Mao, L. Pei, H. Yu, J. Zhang, M.J. Liu, J.S. Zhong, High sensitivity and multicolor tunable optical thermometry in Bi^{3+}/Eu^{3+} co-doped $Ca_2Sb_2O_7$ phosphors, Mater. Today Chem. 27 (2023) 101264.
[33] L. Li, Y.L. Zhu, X.H. Zhou, C.D.S. Brites, D. Ananias, Z. Lin, F.A.A. Paz, J. Rocha, W. Huang, L.D. Carlos, Visible-light excited luminescent thermometer based on single lanthanide organic frameworks, Adv. Funct. Mater. 26 (2016) 8677–8684.
[34] D. Dexter, J. Schulman, The theory of concentration quenching in inorganic phosphors, J. Chem. Phys. 22 (1954) 1063–1070.

[35] X.Y. Huang, S.Y. Wang, J. Liang, B. Devakumar, Eu^{3+}-activated Ca_2YTaO_6 double-perovskite compound: A novel highly efficient red-emitting phosphor for near-UV-excited warm w-LEDs, J. Lumin. 226 (2020) 117408.
[36] Q. Cheng, F.Q. Ren, Q. Lin, H. Tong, X.S. Miao, High quantum efficiency red emitting α-phase $La_2W_2O_9$:Eu^{3+} phosphor, J. Alloys Compd. 772 (2019) 905–911.
[37] M.J. Liu, B. Shen, K.Y. Wang, J.S. Zhong, D.Q. Chen, Highly efficient red-emitting Ca_2YSbO_6:Eu^{3+} double perovskite phosphors for warm WLEDs, RSC Adv. 9 (2019) 20742.
[38] L.J. Zhou, W.X. Wang, D.K. Xu, Z.Y. Wang, Z.B. Yi, M. Wang, Z.G. Lu, Anti-thermal quenching of Eu^{3+} luminescence in negative thermal expansion $Zr(WO_4)_2$, Ceram. Int. 47 (2021) 34820–34827.
[39] K. Ding, A. SR, S. Pang, L.Y. Shan, Y.Q. Zhang, P.F. Sun, B. Deng, R.J. Yu, A potential red-emitting phosphor Ca_2YTaO_6:Eu^{3+}: Luminescence properties, thermal stability and applications for white LEDs, J. Rare Earths 39 (2021) 749–756.
[40] R. Vijayakumar, B. Devakumar, G. Annadurai, H. Guo, X. Huang, Novel high color purity and thermally stable Eu^{3+} ions activated $Ba_2Gd_5B_5O_{17}$ red emitting phosphor for near-UV based WLEDs, Opt. Mater. 84 (2018) 312–317.
[41] Q. Zhu, S. Wang, J.G. Li, X.D. Li, X.D. Sun, Spherical engineering and space-group dependent luminescence behavior of YBO_3:Eu^{3+} red phosphors, J. Alloys Compd. 731 (2018) 1069–1079.
[42] K.T. Liu, H.L. Chen, M.T. Tsai, Y.S. Chang, Preparation and photoluminescence properties of Eu^{3+} ion-doped Mg_2LaTaO_6 phosphor, Microsyst. Technol. 24 (2018) 4043–4048.
[43] Q.N. Mao, B. Shen, T. Yang, J.S. Zhong, G.Q. Wu, A double perovskite-based red-emitting phosphor with robust thermal stability for warm WLEDs, Ceram. Int. 46 (2020) 19328–19334.
[44] H. Guo, X.Y. Huang, Y.J. Zeng, Synthesis and photoluminescence properties of novel highly thermal-stable red-emitting $Na_3Sc_2(PO_4)_3$:Eu^{3+} phosphors for UV-excited white-light-emitting diodes, J. Alloys Compd. 741 (2018) 300–306.
[45] L.L. Devi, C.K. Jayasankar, Spectroscopic investigations on high efficiency deep red-emitting Ca_2SiO_4:Eu^{3+} phosphors synthesized from agricultural waste, Ceram. Int. 44 (2018) 14063–14069.
[46] Q.F. Tang, T. Yang, H.F. Huang, J.Q. Ao, B.Y. Peng, B. Guo, A novel near-ultraviolet–light excitable Eu^{3+}-doped Sr_2LaTaO_6 red phosphor for white-light-emitting diodes, Optik 240 (2021) 166908.
[47] N. Liu, J.Y. Si, G.M. Cai, Y. Tao, Crystal structure, luminescence properties and energy transfer of Eu^{3+}/Dy^{3+} doped $GdNbTiO_6$ broad band excited phosphors, RSC Adv. 6 (2016) 50797.
[48] G.M. Song, M.Z. Li, S.Z. Zhang, N.Z. Wang, P.F. Gong, Z.G. Xia, Z.S. Lin, Enhancing photoluminescence quantum yield in 0D metal halides by introducing water molecules, Adv. Funct. Mater. 30 (2020) 2002468.
[49] S. Ogawa, T. Wakayama, H. Watanabe, K. Hayashi, S. Ogata, Y. Oaki, M. Hasegawa, H. Imai, Enhanced quantum yield of fluorophores in confined spaces of supermicroporous silicas, Bull. Chem. Soc. Jpn. 91 (2018) 87–91.
[50] P. Halappa, H.M. Rajashekar, C. Shivakumara, Synthesis and structural characterization of orange red light emitting Sm^{3+} activated BiOCl phosphor for WLEDs applications, J. Alloys Compd. 785 (2019) 169–177.
[51] Y.B. Hua, W.G. Ran, J.S. Yu, Advantageous occupation of Europium(III) in the B site of double-perovskite $Ca_2BB'O_6$ (B = Y, Gd, La; B′ = Sb, Nb) frameworks for white-light-emitting diodes, ACS Sustainable Chem. Eng. 9 (2021) 7960–7972.
[52] S. Bhushan, M.V. Chukichev, Temperature dependent studies of cathodoluminescence of green band of ZnO crystals, J. Mater. Sci. Lett. 7 (1988) 319–321.
[53] Z.J. Zhang, L.L. Sun, B. Devakumar, G. Annadurai, J. Liang, S.Y. Wang, Q. Sun, X.Y. Huang, Synthesis and photoluminescence properties of a new blue-light-excitable red phosphor Ca_2LaTaO_6:Eu^{3+} for white LEDs, J. Lumin. 222 (2020) 117173.
[54] T. Sakthivel, G. Annadurai, R. Vijayakumar, X.Y. Huang, Synthesis, luminescence properties and thermal stability of Eu^{3+}-activated $Na_2Y_2B_2O_7$ red phosphors excited by near-UV light for pc-WLEDs, J. Lumin. 205 (2019) 129–135.
[55] Q. Liu, L.X. Wang, W.T. Huang, X.B. Li, M.X. Yu, Q.T. Zhang, Thermally stable double perovskite $CaLaMgSbO_6$:Eu^{3+} phosphors as a tunable LED-phosphor material, Ceram. Int. 44 (2018) 1662–1667.
[56] Q. Zhang, X.C. Wang, X. Ding, Y.H. Wang, A potential red-emitting phosphor $BaZrGe_3O_9$:Eu^{3+} for WLED and FED applications: Synthesis, structure, and luminescence properties, Inorg. Chem. 56 (2017) 6990–6998.
[57] H.S. Jang, Y.H. Won, D.Y. Jeon, Improvement of electroluminescent property of blue LED coated with highly luminescent yellow-emitting phosphors, Appl. Phys. B 95 (2009) 715–720.